Journal of Controlled Release 374 (2024) 140–153

Contents lists available at ScienceDirect

Journal of Controlled Release

journal homepage: www.elsevier.com/locate/jconrel

Modified montmorillonite armed probiotics with enhanced on-site mucus-depleted intestinal colonization and H_2S scavenging for colitis treatment

Jiali Yang [b,c,1], Shengchan Ge [c,1], Shaochong Tan [c], Hua Liu [c], Mingzhu Yang [c], Wei Liu [c], Kaixiang Zhang [c], Zhenzhong Zhang [c], Junjie Liu [c], Jinjin Shi [c,*], Zhi-Hao Wang [c,*], Jitian Li [a,*]

[a] Henan Luoyang Orthopedic Hospital (Henan Provincial Orthopedic Hospital), 100 Yongping Road, Zhengzhou 450000, China
[b] Institute of Brain Science and Disease, School of Basic Medicine, Shandong Provincial Key Laboratory of Pathogenesis and Prevention of Neurological Disorders, Qingdao University, Qingdao 266021, PR China
[c] School of Pharmaceutical Sciences, Zhengzhou University, Zhengzhou 450001, PR China

ARTICLE INFO

Keywords:
Inflammatory bowel disease
Probiotics colonization
Montmorillonite
Depleted mucus
Hydrogen sulfide

ABSTRACT

Inflammatory bowel diseases (IBD) are often associated with dysregulated gut microbiota and excessive inflammatory microenvironment. Probiotic therapy combined with inflammation management is a promising approach to alleviate IBD, but the efficacy is hindered by the inferior colonization of probiotics in mucus-depleted inflammatory bowel segments. Here, we present modified montmorillonite armed probiotic *Escherichia coli* Nissle 1917 (MMT-Fe@EcN) with enhanced intestinal colonization and hydrogen sulfide (H_2S) scavenging for synergistic alleviation of IBD. The montmorillonite layer that can protect EcN against environmental assaults in oral delivery and improve on-site colonization of EcN in the mucus-depleted intestinal segment due to its strong adhesive capability and electronegativity, with a 22.6-fold increase in colonization efficiency compared to EcN. Meanwhile, MMT-Fe@EcN can manage inflammation by scavenging H_2S, which allows for enhancing probiotic viability and colonization for restoring the gut microbiota. As a result, MMT-Fe@EcN exhibits extraordinary therapeutic effects in the dextran sulfate sodium-induced mouse colitis models, including alleviating intestinal inflammation and restoring disrupted intestinal barrier function, and gut microbiota. These findings provide a promising strategy for clinical IBD treatment and potentially other mucus-depletion-related diseases.

1. Introduction

Inflammatory bowel diseases (IBD) have become a significant global health concern, affecting millions of individuals worldwide [1]. Emerging evidence suggests that IBD is associated with the disturbance in the bacterial microbiota and dysfunction of the intestinal mucosal barrier, subsequently leading to an overactivated inflammatory environment in the intestinal tracts and exposing patients to chronic systemic inflammation in the long term [2]. Currently, available clinical therapies are mostly focused on improving disease-related symptoms by using small-molecule drugs to suppress the intestinal inflammatory burden, while suffering from limited treatment benefits. Oral probiotic therapeutics, by resting on the gut to positively modulate the balance of bacterial composition and to promote intestinal mucosal repair, have been promising approaches to alleviate IBD by combining with inflammation management [3–8], with several probiotics currently being evaluated in clinical trials (ClinicalTrials.gov ID NCT05652621 and NCT03266484) [9]. Unfortunately, probiotic therapeutics are hindered by the challenges of achieving sufficient colonization efficiency, especially in conditions where the mucus layer is depleted in the pathological intestinal tracts of IBD. The mucus layer normally provides a natural habitat for probiotics to colonize [10,11], but its depletion during

* Corresponding authors.
E-mail addresses: shijinyxy@zzu.edu.cn (J. Shi), wangzhihao@zzu.edu.cn (Z.-H. Wang), jitianlee@hotmail.com (J. Li).

[1] Jiali Yang and Shengchan Ge both equally contributed to this study. Jiali Yang, Shengchan Ge, Shaochong Tan, Hua Liu, and Mingzhu Yang performed experimental measurements. Wei Liu and Kaixiang Zhang provided Technical support. Zhenzhong Zhang, Junjie Liu, Jinjin Shi, Zhi-Hao Wang, and Jitian Li contributed to the data interpretation and provided financial support.

https://doi.org/10.1016/j.jconrel.2024.07.071
Received 2 April 2024; Received in revised form 8 July 2024; Accepted 29 July 2024
Available online 14 August 2024

inflammation poses significant hurdles for probiotic colonization and therapeutic efficacy.

Recent advances in biofilms [12], hydrogels [13], and nanocoatings [14] have shown promise in enhancing the probiotic delivery and adhesion within the intestinal mucus. However, current methods mainly focus on enhancing interactions with intestinal mucus, and their efficacy may be limited under conditions of sustained mucus depletion and complex pathological microenvironments during IBD. Furthermore, the excessive production of hydrogen sulfide (H_2S) in the inflamed sites further depleted the mucus layer, which is detrimental to both probiotic colonization and the recovery from IBD [15–17]. H_2S can break the disulfide bonds of the mucin polymers in the mucus that attenuate the viscosity and promote the permeability of mucus [18,19]. The mucus layer is the site of colonization of intestinal microorganisms [10], and there is no doubt that intestinal barrier damage is not conducive to probiotic adhesion. As the understanding of gut microbiota dysbiosis and its impact on IBD deepens, the development of new and effective approaches that enhance probiotic colonization in mucus-depleted inflamed lesion sites holds great clinical significance. Addressing this challenge could lead to significant improvements in the treatment and management of IBD, providing hope for better outcomes and improved quality of life for patients.

To fulfil this demand, Fe^{3+}-containing montmorillonite nanotablets (MMT-Fe)-armed *Escherichia coli* Nissle 1917 (EcN) have been established to achieve efficient IBD treatment via enhanced on-site mucus-depleted intestinal colonization and H_2S scavenging (Scheme 1). Specifically, montmorillonite coating enhanced the colonization of EcN in mucus-depleted inflammatory bowel segments via strong adhesive capability and electronegativity. Furthermore, it can act as a guardians of EcN, a strain with an established history of human safety and efficacy in maintaining remission of ulcerative colitis, protecting these encapsulated probiotics from damage in the gastrointestinal environment, thereby rapidly orienting barrier function and the gut microbiota to a beneficial state. Additionally, MMT-Fe@EcN plays a pivotal role in the reduction of H_2S concentration and the restoration of the compromised mucus layer at inflamed sites. In the dextran sulfate sodium (DSS)-induced colitis, MMT-Fe@EcN improved the probiotic colonization efficiency, rapidly repaired the intestinal barrier, reduced clinical disease scores, and restored intestinal microenvironment, providing a promising strategy for enhancing the bacteriotherapy of clinical IBD.

2. Results

2.1. Preparation and characterization of MMT-Fe@EcN

The development of probiotic coating materials aimed at enhancing efficient colonization within the mucus-depleted segment of the intestine is crucial for restoring the gut microbiota. Montmorillonite (MMT) is a natural negatively-charged layered material, which is well tolerated by the digestive tract and has been clinically used to alleviate diarrhea through physical binding, covering of mucosa, and removal of toxins, emerges as a promising candidate for efficient probiotic armament. MMT can be exfoliated into nanosheets upon application of appropriate mechanical forces [20], and we obtained nanoscale montmorillonite suspensions by stirring and ultrasonic dispersion, thereby increasing its surface area and its ability to adsorb and encapsulate probiotics. Moreover, capitalizing on its exceptional adsorption and ion exchange properties, we have engineered Fe^{3+}-containing montmorillonite nanosheets (MMT-Fe), as depicted in Fig. 1A, which not only facilitates physical adsorption but also chemical consumption of H_2S [21,22]. Transmission electron microscopy (TEM) images revealed that MMT-Fe exhibited irregular or rough sheet-like structures. Furthermore, energy-dispersive X-ray spectroscopy (EDX), X-ray photoelectron spectroscopy (XPS), and ICP-MS analysis demonstrated the successful loading of Fe onto MMT, with iron loading of 8 wt% (Fig. 1B,C and Fig. S1–2). The infrared (IR) spectra and X-ray diffraction (XRD) analysis proved that the incorporation of Fe did not affect the main structure of montmorillonite [23] (Fig. 1D,E).

Subsequently, MMT-Fe was harnessed as the coating material for the oral delivery *Escherichia coli* Nissle 1917 (EcN). EcN, a well-known probiotic bacterium, which has been widely used for treating a range of gastrointestinal disorders and metabolic diseases. EcN can inhibit the proliferation of harmful bacteria in the intestine and promote the growth of beneficial bacteria, thus maintaining the homeostasis of intestinal microbes [24–28]. The optimal feed ratio and synthesis time were determined by flow cytometry and CLSM (Fig. S3–6). The MMT-Fe coating on the 1×10^8 CFU EcN surface was analyzed by ICP-MS at approximately 1.73 mg(Fig. S7). TEM images showed that EcN were successfully encapsulated in the MMT-Fe coating (Fig. 1F). Scanning electron microscopy (SEM) images confirmed that MMT-Fe@EcN exhibited a significantly higher contrast and rough surface compared to EcN (Fig. 1G). Additionally, EDX analysis clearly demonstrated the distribution of O, Si, Al, and Fe signals, further confirming the encapsulation of EcN within MMT-Fe (Fig. 1H). Furthermore, by labeling the MMT-Fe coating with Rhodamine B, flow cytometry histograms showed a significantly increased fluorescence intensity compared to EcN, with an encapsulation efficiency of 93.4% (Fig. 1I). Confocal laser scanning microscopy (CLSM) imaging results displayed a high degree of colocalization between the bacteria expressing green fluorescence and the Rhodamine B-stained coating (Fig. 1J). Dynamic light scattering (DLS) results revealed that the diameter of EcN was approximately 884.3 ± 98.2 nm, while the diameter of MMT-Fe@EcN was approximately

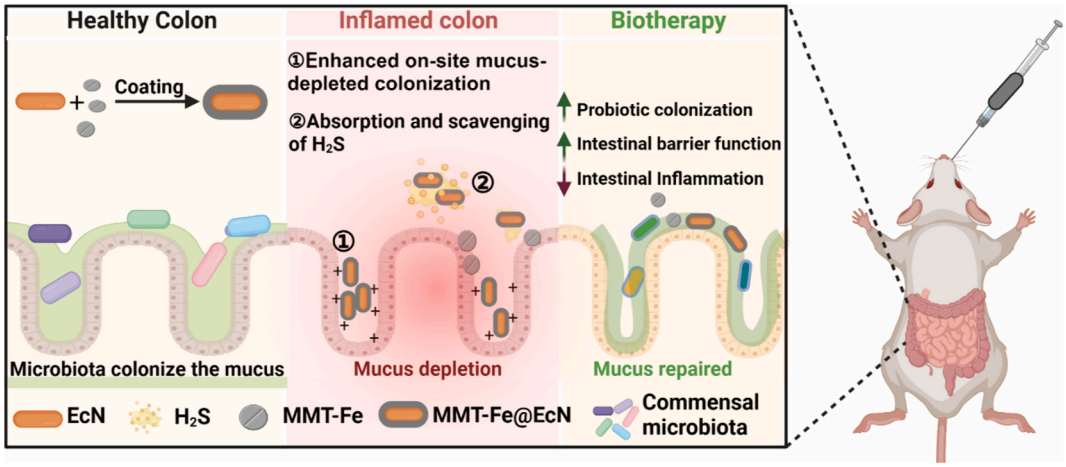

Scheme 1. Schematic diagram of the mechanism of MMT-Fe@EcN treatment for colitis.

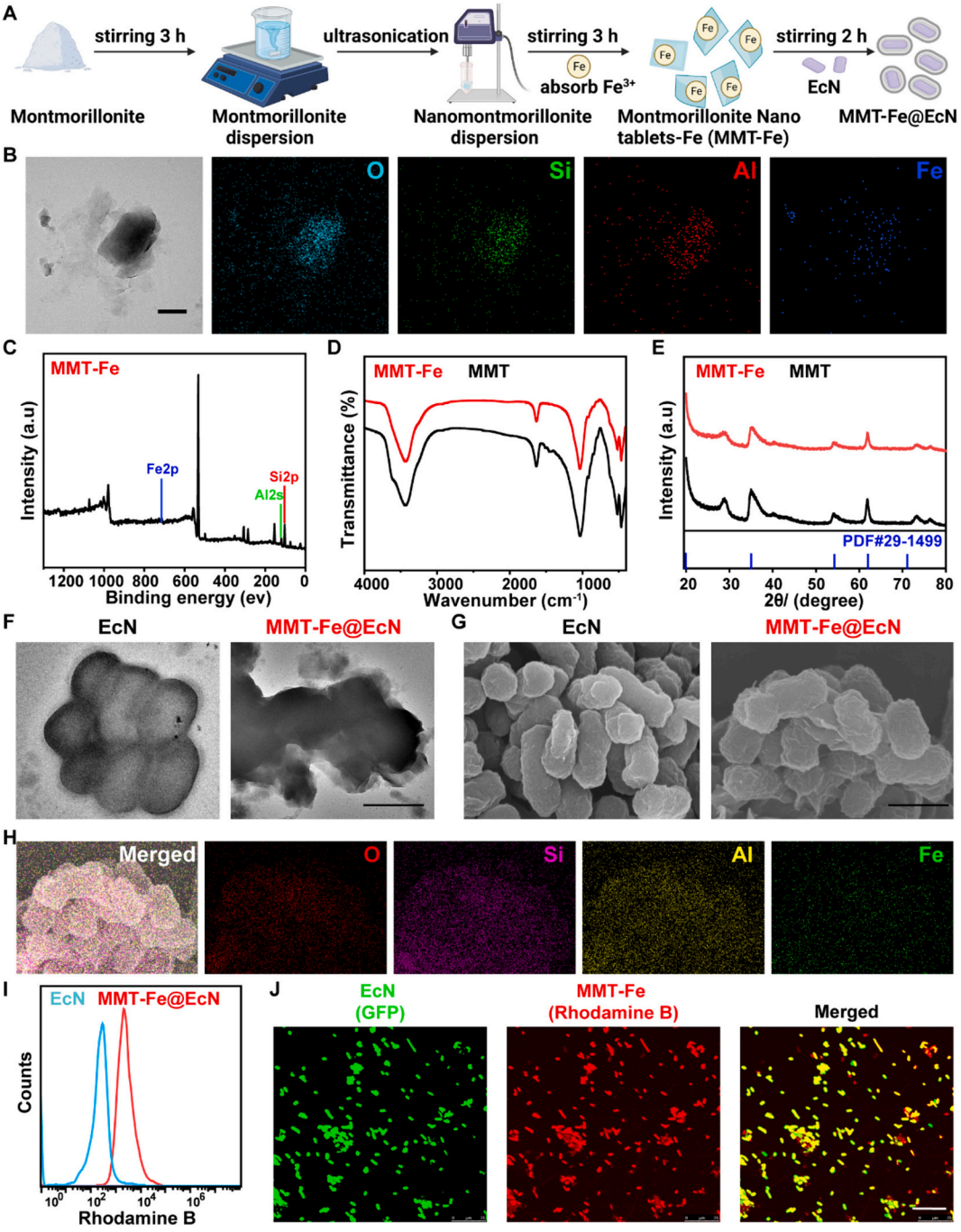

Fig. 1. Preparation and Characterization of MMT-Fe@EcN. A) The diagram illustrates the synthesis process of MMT-Fe@EcN. B) Representative TEM and HAADF-STEM images of MMT-Fe. The elemental distribution is visualized with colors: O (turquoise), Si (green), Al (red), and Fe (blue). Scale bar, 200 nm. C) XPS spectra of MMT-Fe. D, E) FT-IR and XRD spectra of MMT-Fe are displayed. F, G) Representative TEM and SEM images of both MMT-Fe@EcN and EcN separately. Scale bar, 1 μm. H) Representative HAADF-STEM images along with element mapping for MMT-Fe@EcN. The elements are distinguished as O (red), Si (purple), Al (yellow), and Fe (green). I) Flow cytometry histograms for Rhodamine B-labeled MMT-Fe@EcN, with native EcN serving as a control. J) CLSM images of MMT-Fe@EcN. The green channel represents the green fluorescent plasmid carried by EcN, while the red channel displays the Rhodamine B-labeled MMT-Fe coating. Scale bar, 25 μm. (For interpretation of the references to colour in this figure legend, the reader is referred to the web version of this article.)

1319.2 ± 22.5 nm. The Zeta potential of EcN was −17.1 ± 1.3 mV, while that of MMT-Fe@EcN was −38.9 ± 2.8 mV (Fig. S8). The abundant negative charges on the MMT-Fe surface resulted in a significant decrease in potential after coating, indicating the successful formation of the coating. To assess whether the MMT-Fe coating affected bacterial viability and growth, we evaluated the growth curve and viability of coated EcN in the culture medium by recording the optical density values at 600 nm and 450 nm, respectively. As shown in Fig. S9, the growth curve and bacterial viability exhibited no significant differences compared to unmodified EcN. These results indicate that the MMT-Fe coating did not negatively impact the viability and growth of the probiotic bacteria.

2.2. Improved resistance of MMT-Fe@EcN to gastrointestinal invasion in vitro

Oral probiotics often encounter harsh conditions in the gastrointestinal tract, which can compromise their activity [29,30]. The water-impermeable property provided by montmorillonite can effectively delay the permeation of gastric acid and bile salts. To validate the protective effect of MMT-Fe on probiotics, EcN and MMT-Fe@EcN were treated with simulated gastric fluid (SGF) and bile salts, and the bacteria's morphology was observed using TEM. The results demonstrated that the coating effectively shielded the probiotics from the assault of SGF and bile salts, preserving the intact bacterial morphology (Fig. S10). Moreover, TEM images indicated that bile salts dissolved the lipid membrane and disrupted the uncoated bacteria, while the coating prevented the penetration of bile salts, thus maintaining the integrity of the MMT-Fe@EcN (Fig. S10). Furthermore, bacterial colony counts were

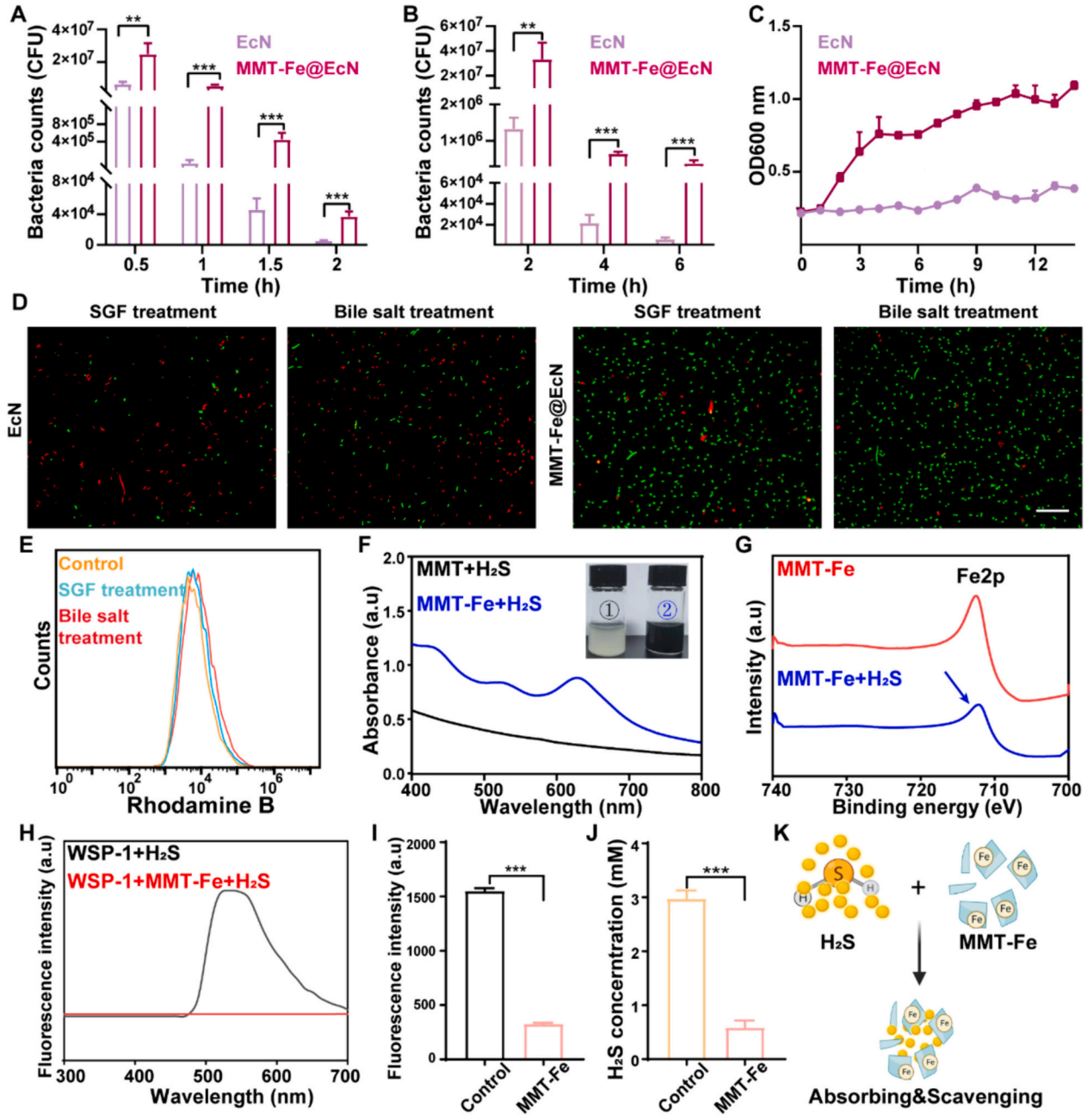

Fig. 2. Enhanced Gastrointestinal Resistance of MMT-Fe@EcN in vitro. Equivalent MMT-Fe@EcN and EcN were exposed to the following: A) SGF for 2 h and B) bile salts for 6 h. Bacterial quantities were determined using plate counting at the indicated time intervals ($n = 3$). C) Growth curves for MMT-Fe@EcN and EcN in LB broth, following treatment with SGF for 1 h and bile salts (0.3 mg mL^{-1}) for 2 h at 37 °C ($n = 3$). OD_{600} measurements were taken at 1-h intervals using a microplate reader. D) The live/dead cell viability assay of MMT-Fe@EcN and EcN after treatment in SGF for 0.5 h and bile salts (0.3 mg mL^{-1}) for 1 h. Living cells are denoted in green, while deceased cells are marked in red. Scale bar, 20 μm. E) Flow cytometry histograms representing bacterial samples after incubation in SGF for 0.5 h and bile salts (0.3 mg mL^{-1}) for 1 h. F) Photographs and absorption spectra depicting the changes in MMT-Fe before and after reacting with H_2S. G) XPS Fe 2p electron level of before and after reaction with H_2S. H, I) Fluorescence spectra and intensity of MMT-Fe before and after reaction with H_2S ($n = 3$). J) H_2S concentrations before and after MMT-Fe treatments (n = 3). K) Schematic representation of H_2S adsorbing and scavenging by MMT-Fe. a.u., arbitrary units. Data are presented as the means ± SD (n = 3). ***$P < 0.001$ determined by Student's *t*-test. **$P < 0.01$, ***$P < 0.001$ determined by Student's *t*-test. (For interpretation of the references to colour in this figure legend, the reader is referred to the web version of this article.)

performed after SGF and bile salts treatment to determine bacterial survival. As shown in Fig. 2A, after 2 h of SGF treatment, the survival rate of MMT-Fe@EcN was 7 times higher than that of EcN. The same trend was observed after bile salt treatment, with MMT-Fe@EcN showing a 61-fold higher survival rate than EcN after 6 h of treatment (Fig. 2B). To further simulate the growth trend of bacteria after exposure to gastrointestinal conditions, the growth curves of bacteria were recorded after consecutive treatment with SGF and bile salts. As depicted in Fig. 2C, MMT-Fe@EcN demonstrated a significant advantage in promoting probiotics growth, displaying an OD_{600} value that was 0.8 higher compared to EcN. A live/dead cell viability assay further assessed bacterial viability under different treatments, showing that many red dead cells were observed in the EcN group, while most MMT-Fe@EcN cells remained alive (Fig. 2D). Lastly, the stability of the coating was investigated, and flow cytometry and CLSM results showed that the coating remained stable on the surface of EcN even after treatment with SGF and bile salts (Fig. 2E and Fig. S11–12). These findings confirm that MMT-Fe can effectively enhance probiotics' resistance to harsh environmental conditions, thereby establishing a robust foundation for their successful colonization in the intestine.

Next, we examined the coating's ability to scavenge H_2S in vitro. The introduction of Fe into the interlayer space of MMT (MMT-Fe) allows for the physical adsorption and chemical consumption of H_2S [21,22]. As a consequence, a noticeable colour change occurred in MMT-Fe, and it exhibited a sharp absorption peak around 660 nm upon reaction with H_2S, resulting in the formation of FeS (Fig. 2F and Fig. S13). Furthermore, the characteristic signals of Fe in MMT-Fe significantly decreased after the addition of H_2S, providing further evidence of the reaction

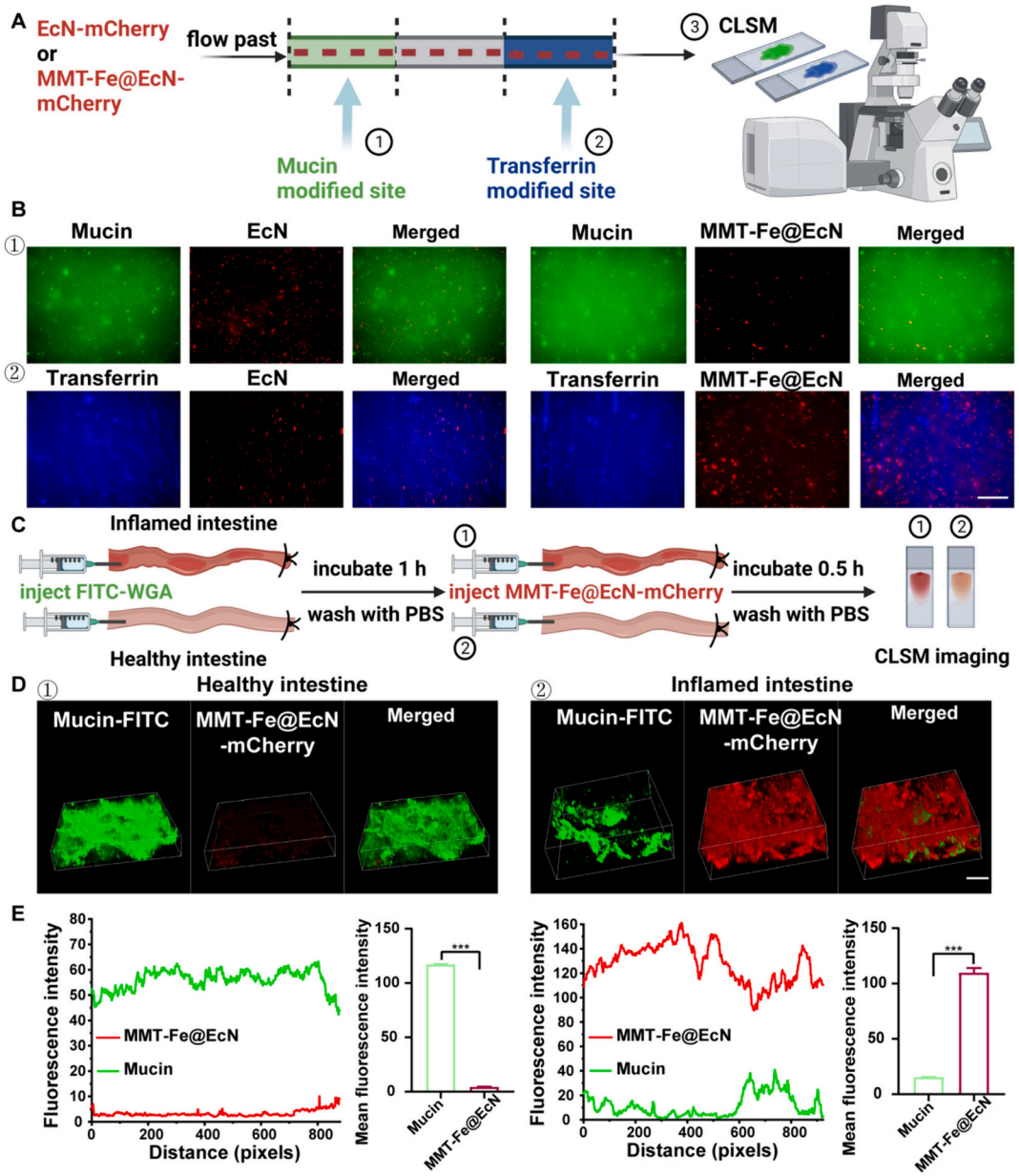

Fig. 3. The lesion-adhesive property of MMT-Fe@EcN at the inflamed site. A) Demonstration of adhesion test protocol on different modified plates. The experimental study involved the surface modification of separate plates with mucin and transferrin, respectively. Following the modification, the plates were subjected to the flow of EcN and MMT-Fe@EcN. B) Representative CLSM images of EcN and MMT-Fe@EcN adhesion on different modified plates. Scale bar, 10 μm. C) Demonstration of adhesion test protocol in vitro. D) Observation of MMT-Fe@EcN adhesion at the mucosal level in healthy and inflamed intestines by CLSM imaging. Scale bar, 20 μm. E) Distribution of MMT-Fe@EcN fluorescence signals and statistical quantitative analysis of CLSM images ($n = 3$). Data are presented as the means ± SD (n = 3). ***$P < 0.001$ determined by Student's *t*-test.

(Fig. 2G). To further investigate the H_2S removal ability of MMT-Fe, a fluorescent probe WSP-1 containing reactive disulfide compounds was utilized. WSP-1 selectively and rapidly reacts with hydrogen sulfide, generating a fluorescent compound that emits characteristic fluorescence under 465 nm excitation [15]. However, the fluorescence disappears in the presence of H_2S and MMT-Fe, indicating successful H_2S removal (Fig. 2H and I). Additionally, an H_2S content detection kit was used to quantitatively measure the adsorption and consumption of H_2S by MMT-Fe, as shown in Fig. 2J. This demonstrated that MMT-Fe can reduce concentrations of H_2S. We further examined whether the MMT-Fe coated probiotic retained its ability to clear H_2S. As shown in Fig. S14, MMT-Fe@EcN significantly reduced the concentration of H_2S compared to the control group, thereby confirming its ability to scavenge H_2S effectively. Together, the incorporation of Fe into the interlayer space of MMT facilitates the formation of FeS upon interaction with H_2S, leading to efficient adsorption and scavenging of H_2S (Fig. 2K).

2.3. The lesion-adhesive property of MMT-Fe@EcN at the inflamed site

The colonization of probiotics in the intestinal tract is essential for their therapeutic efficacy [31,32]. However, in the context of intestinal inflammation, the damaged mucus layer significantly hinders probiotic colonization [30]. IBD is characterized by local intestinal lesions, where immune cells accumulate and secrete positively charged pro-inflammatory factors, leading to a reversal of the electric potential and resulting in a positive luminal side [33,34]. According to zeta potential measurements, EcN carried a negative charge due to their cell wall characteristics, while MMT-Fe@EcN exhibited a higher negative charge as MMT-Fe was negatively charged (Fig. S15). Therefore, we hypothesized that MMT-Fe@EcN could improve the adhesion ability of probiotics at the site of inflammation. To validate this hypothesis, a plate was modified with mucin (labeled with FITC, green fluorescence, in the healthy intestine) and transferrin (labeled with Cy5, blue fluorescence, increased expression in the inflamed intestine [35]) and then simulated intestinal peristalsis by flowing MMT-Fe@EcN and EcN (carrying mCherry plasmid, red fluorescence) through the plate (Fig. 3A). As shown in Fig. 3B, on the plate modified with transferrin to simulate an inflammatory environment, the fluorescence of MMT-Fe@EcN adhering to the plate was 5 times higher than that of the mucin group, indicating that MMT-Fe@EcN may retain a significantly higher level of adhesion under colonic inflammation conditions.

Further investigation of the specific location of MMT-Fe@EcN adherence in the colonic mucosa was conducted by injecting bacteria into ex vivo intestinal tissue and staining the mucus layer (stained with wheat germ agglutinin-FITC, green) (Fig. 3C). The distribution and location of MMT-Fe@EcN in the mucosal layer were observed through CLSM. As shown in Fig. 3D, there was a noticeable fluorescent signal of MMT-Fe@EcN in the inflamed intestine group, whereas the healthy intestine group showed no such a strong signal. Furthermore, the fluorescence signal of the MMT-Fe@EcN was stronger in the lesion site (23.9 times higher) where the mucosal fluorescence signal was relatively low, indicating that MMT-Fe@EcN may aggregate at the site of injury and provide a bridge for the colonization of probiotics (Fig. 3E). The results confirmed that MMT-Fe@EcN exhibited prolonged retention in the inflamed colon, enhanced adhesion at the lesion site, and facilitated the colonization of probiotics at the diseased site.

2.4. Enhanced colonization of MMT-Fe@EcN in colitis

Having confirmed the adhesion and retention of MMT-Fe@EcN under simulated inflammatory colonization conditions in vitro, we proceeded to validate its potential to enhance probiotic colonization in vivo. For this purpose, healthy mice and colitis-induced mice were orally administered with 1×10^8 CFU of MMT-Fe@EcN or EcN, and colonic tissues were collected for observation of bacterial colonization through TEM (Fig. 4A). As shown in Fig. 4B, MMT-Fe@EcN enhanced the colonization of probiotics at the inflamed site, which aligns with the in vitro results obtained in Fig. 3. To observe the transit of MMT-Fe@EcN through the gastrointestinal tract, in vivo animal imaging was employed. As shown in Fig. 4C,D, the fluorescence intensity of MMT-Fe@EcN in the intestines of colitis-induced mice was higher than that of the EcN group, suggesting an augmented retention and adhesion of MMT-Fe@EcN within the intestine.

Moreover, to quantify the quantity of adhered and colonized probiotics in the gastrointestinal tract, plate counting was performed. The results demonstrated a significantly higher count of MMT-Fe@EcN in the intestine compared to EcN. Additionally, the survival rate of MMT-Fe@EcN in the mice's stomach was nearly 7.5 times that of EcN (Fig. 4E). Notably, at 4 h after oral administration, the number of MMT-Fe@EcN in the colon was approximately 6 times higher than that of EcN (Fig. 4E). Similar results were obtained at 48 and 96 h, with MMT-Fe@EcN being approximately 5.2 times and 22.6 times higher than the EcN group, respectively (Fig. 4E). Despite the inevitable decrease in probiotic concentration over time due to mucus layer renewal and intestinal emptying, our findings demonstrate that the survival rate of MMT-Fe@EcN in vivo was significantly higher than that of EcN alone. Furthermore, the long-term adhesion of MMT-Fe@EcN was observed through frozen sections, revealing the persistence of MMT-Fe@EcN in the intestines even after a 6-day oral gavage, while the signal of EcN had disappeared (Fig. 4F). This result strongly confirms the long-term adhesion and colonization of MMT-Fe@EcN in the gastrointestinal tract. Importantly, no side effects were observed from the oral administration of MMT-Fe@EcN, the hematology and blood biochemistry did not exhibit abnormalities compared to the control group (Fig. S16). Additionally, hematoxylin and eosin (H&E) staining demonstrated that on the 5th day after oral administration, the intestinal tissues did not exhibit histological damage or morphological differences compared to the control group (Fig. S17).

2.5. MMT-Fe@EcN exerted a powerful therapeutic effect on DSS-colitis

DSS-induced colitis is one of the most commonly used animal models to simulate IBD [36]. We evaluated the therapeutic efficacy of MMT-Fe@EcN in DSS-induced colitis and the experimental flow chart is shown in Fig. 5A. Notably, the DSS group showed a significant reduction in body weight, while the MMT-Fe@EcN group exhibited weight recovery and alleviated inflammation (Fig. 5B). Disease activity index (DAI) scores were measured to assess the severity of colitis based on weight loss, stool consistency, and fecal bleeding [37]. Compared to the DSS group, the DAI scores of the EcN, MMT-Fe and EcN were administered orally separately (MMT-Fe + EcN), and MMT-Fe@EcN groups decreased by 47.3%, 50.0%, and 71.0%, respectively, confirming that MMT-Fe@EcN was the most effective in alleviating the severity of colitis (Fig. 5C). Moreover, the length of colonic inflammation damage in the DSS group (4.9 ± 0.4 cm) was significantly reduced, and the MMT-Fe@EcN group (7.1 ± 0.6 cm) showed a significant recovery in colon length compared to the EcN group (6.2 ± 0.2 cm) and MMT-Fe + EcN group (6.2 ± 0.4 cm) (Fig. 5D,E). Importantly, the concentration of H_2S in the feces of mice in the MMT-Fe@EcN group (4.6 ± 1.4 μM) was similar to that of healthy mice (4.7 ± 1.6 μM), significantly lower than the DSS group (14.6 ± 1.6 μM), EcN group (12.33 ± 2.3 μM), and MMT-Fe + EcN group (8.27 ± 2.3 μM) (Fig. 5F). Excessive H_2S in the intestinal environment promotes the development of IBD by disrupting the epithelial barrier [17,38], and the clearance of H_2S helps restore the intestinal barrier and promote the recovery of IBD [15]. Compared to the EcN and MMT-Fe + EcN groups, the MMT-Fe@EcN group significantly reduced the systemic exposure of orally administered fluorescein isothiocyanate (FITC)-dextran after DSS treatment ($P < 0.001$, Fig. 5G), indicating a significant restoration of intestinal barrier function. Immunofluorescence staining images visually demonstrated that MMT-Fe@EcN normalized the expression patterns of occludin-1 and ZO-1 in DSS-induced colitis mice, two tight junction-associated proteins critical

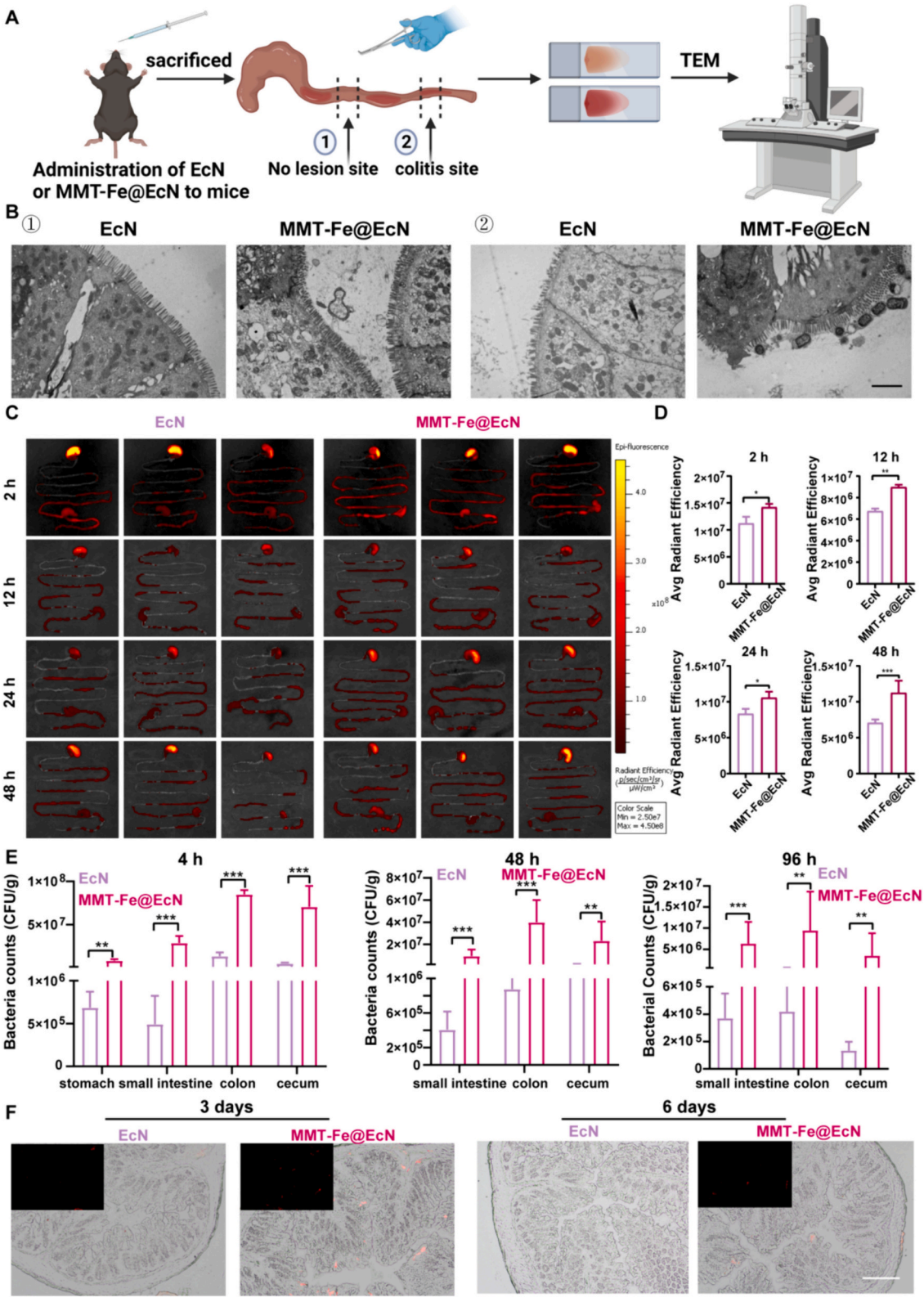

Fig. 4. Enhanced colonization of MMT-Fe@EcN in colitis. A) Demonstration of intestinal adhesion assay protocols in healthy mice and colitis mice. B) Representative colon TEM images of healthy and colitis mice. Scale bar, 2 μm. C) IVIS images of the gastrointestinal tracts collected at 2, 12, 24, and 48 h post-administration of either EcN or MMT-Fe@EcN. D) Statistical quantitative analysis of IVIS images (n = 3). E). Enumeration of bacteria in the intestine, colon, and cecum at 4 h, 48 h, and 96 h following oral administration, respectively (n = 3). F) Long-term in vivo intestinal adhesion of EcN and MMT-Fe@EcN. Representative images of colon sections on days 3 and 6 after a single gavage dose were captured using CLSM. Scale bar, 100 μm. Data are presented as the means ± SD (n = 3). $^{*}P < 0.05$, $^{**}P < 0.01$, $^{***}P < 0.001$ determined by Student's *t*-test.

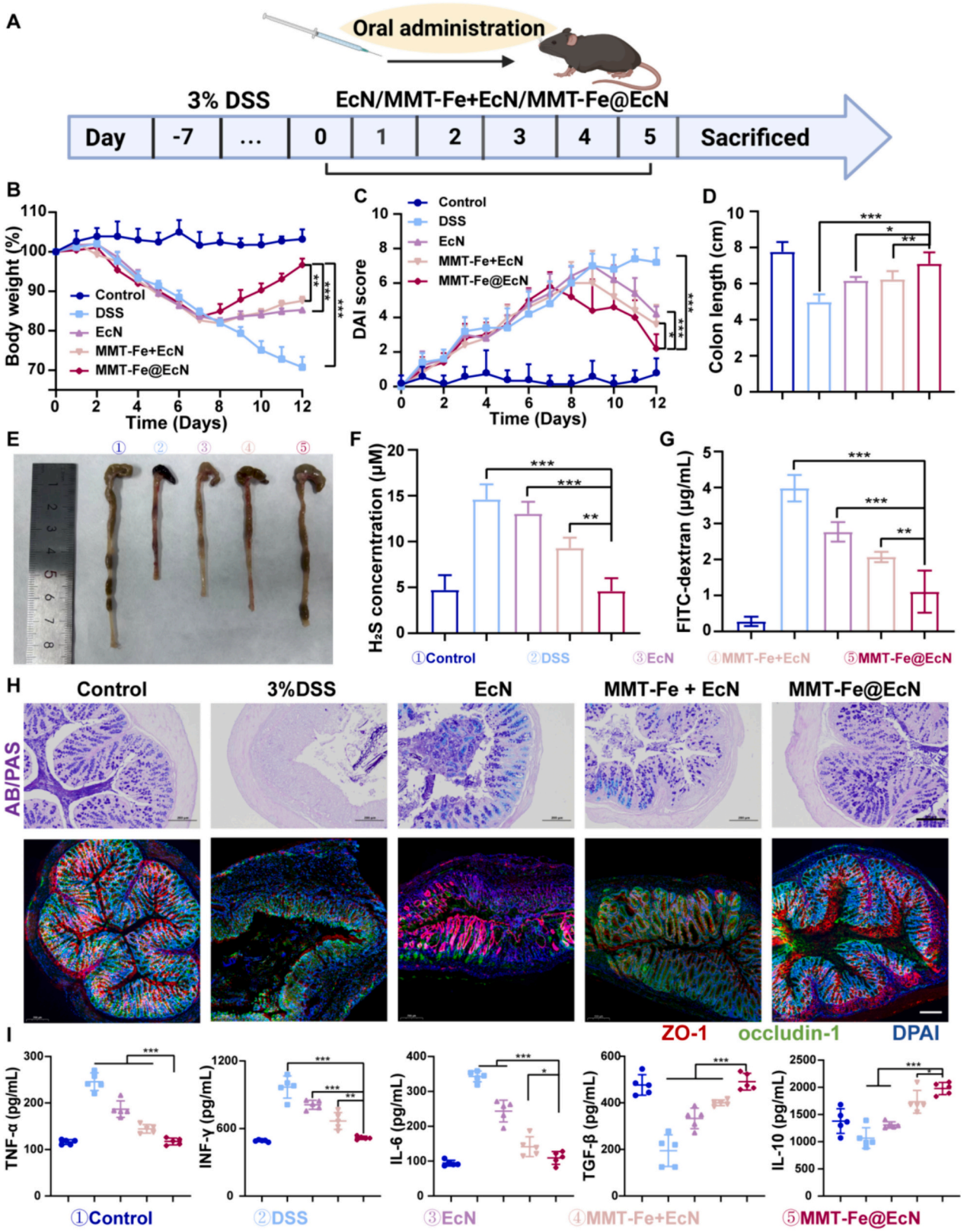

Fig. 5. MMT-Fe@EcN exerts a powerful therapeutic effect in DSS-colitis. A) A schematic representation of the entire procedure for establishing the DSS-induced colitis mouse model and subsequent oral treatment administration. B) The body weight of the mice was monitored throughout the 12-day experiment. C) DAI score values recorded over the course of 12 days in the experiment. D) The corresponding lengths and E) photographs of the excised colons from the specified experimental groups. F) H_2S concentrations in each group. (n = 3). G) On the 12th day, an assessment of intestinal barrier function was conducted in vivo within each group of mice through the oral administration of 4 kDa FITC-dextran. Fluorescence intensity in the serum was measured 4 hours later. H) Display of representative images of AB/APS, ZO-1, and occludin-1 staining in the colons of mice from each group. Scale bar, 100 μm. I) On the 12th day, levels of pro and anti-inflammatory cytokines in colonic tissue were analyzed ($n = 5$). Data are presented as the means ± SD (n = 5). $^{*}P < 0.05$, $^{**}P < 0.01$, $^{***}P < 0.001$ determined by Student's *t*-test.

for intestinal homeostasis [39]. However, other groups, including the EcN and MMT-Fe + EcN groups, showed minimal effects (Fig. 5H and Fig. S18). Alcian blue/periodic acid Schiff (AB/PAS) staining images also revealed that MMT-Fe@EcN treatment significantly restored the mucus layer, similar to the healthy group (Fig. 5H).

Furthermore, colonic H&E staining sections (Fig. S19) and terminal deoxynucleotidyl transferase dUTP nick end labeling (TUNEL) (Fig. S20) analysis indicated that MMT-Fe@EcN reduced colonic epithelial cell damage and apoptosis levels. Surprisingly, MMT-Fe@EcN treatment significantly reduced the levels of local pro-inflammatory cytokines, such as IL-6, TNF-α, and IFN-γ, while increasing the levels of the anti-inflammatory cytokines IL-10 and TGF-β (Fig. 5I). Importantly, the ROS levels in the MMT-Fe@EcN group were significantly lower than those in the DSS model group, EcN group, and MMT-Fe + EcN group, indicating that MMT-Fe@EcN effectively cleared ROS and reduced intestinal inflammation after reaching the site of colitis (Fig. S21). Myeloperoxidase (MPO), an enzyme associated with neutrophils in inflammatory tissues and the mucosa and submucosa of inflamed tissue, was significantly reduced after MMT-Fe@EcN treatment (Fig. S22). We further evaluated the efficacy of MMT-Fe, and the results demonstrated that while MMT-Fe had some therapeutic efficacy, MMT-Fe@EcN was significantly superior in treating colitis (Fig. S23). In summary, these results demonstrate that MMT-Fe@EcN has a strong therapeutic effect in a mouse model of DSS-induced colitis compared to using EcN, MMT-Fe or MMT-Fe + EcN.

Additionally, further investigation of bacterial translocation was carried out. The heart, liver, spleen, lungs, and kidneys were extracted and homogenized with PBS. Subsequently, 50 μL of each suspension was plated on LB agar plates containing antibiotics and incubated overnight at 37 °C for colony counting. As shown in Fig. S24, both the EcN-mCherry group and the MMT-Fe + EcN-mCherry group exhibited significant adverse effects with bacterial translocation to distant tissues, whereas the coating on MMT-Fe@EcN-mCherry effectively prevented bacterial translocation.

Finally, we also conducted a preventive study according to the design shown in Fig. S25. The results showed that MMT-Fe@EcN treatment in DSS-induced colitis mice rapidly restored body weight and resulted in colon length closer to that of healthy mice. Additionally, MMT-Fe@EcN protected the colonic epithelium from pathological damage and significantly restored the intestinal mucus layer barrier compared to the DSS model group, EcN group, and MMT-Fe + EcN group. In conclusion, MMT-Fe@EcN treatment demonstrated good therapeutic and preventive effects in a mouse model of colitis.

2.6. MMT-Fe@EcN restores colitis-associated gut microbiota dysbiosis

The dysbiosis of the gut microbiota plays a crucial role in the development of IBD [40–42]. Encouraged by the satisfactory therapeutic outcomes mentioned earlier, we proceeded to evaluate whether MMT-Fe@EcN regulates the composition of the gut microbiota in mice with colitis. To ensure robust data analysis, we first conducted a Species Accumulation Boxplot analysis, confirming the sufficiency of the sample size (Fig. 6A). The Venn diagram further illustrated the composition of the gut microbiota in each group. After removing 364 shared features among the five groups, Control, DSS, EcN, MMT-Fe + EcN, and MMT-Fe@EcN had 102, 47, 36, 36, and 83 unique feature sequences, respectively (Fig. 6B). To further assess the differences in microbiota composition between samples, we employed β-diversity analysis. Non-Metric Multi-Dimensional Scaling (NMDS) analysis demonstrated that the MMT-Fe@EcN-treated group clustered more closely to the healthy control group, compared to the other treatment groups, suggesting that MMT-Fe@EcN treatment reestablished a healthier microbiota (Fig. 6C). This result was further supported by UPGMA clustering analysis, which showed similarities between the MMT-Fe@EcN-treated group and the healthy control group, indicating a positive regulatory effect of MMT-Fe@EcN on the gut microbiota (Fig. 6D).

Additionally, we analyzed the taxonomic composition of the microbiota in different treatment groups and presented the top 10 species at the Family level based on relative abundance in bar graphs (Fig. 6E). In IBD, certain pathogenic bacteria, such as sulfate-reducing bacteria that produce H_2S, contribute to intestinal inflammation. Remarkably, we observed a significant reduction in the abundance of sulfate-reducing bacteria, including Bilophila and Desulfovibrio, in mice treated with MMT-Fe@EcN compared to the other treatment groups (Fig. 6F). Furthermore, the dysbiotic expansion of Enterobacteriaceae during intestinal inflammation also significantly decreased after MMT-Fe@EcN treatment, indicating the potential of MMT-Fe@EcN therapy in ameliorating the detrimental effects of microbiota dysbiosis during gut inflammation (Fig. 6F). Of particular interest, we noted a significant increase in *Akkermansia muciniphila*, a bacteria associated with a protective gut barrier function, after MMT-Fe@EcN treatment, compared to the other treatment groups (Fig. 6F). Finally, to assess the differences in dominant species between different samples, we utilized a ternary plot (species-level) and conducted an LDA effect size analysis. These analyses visually demonstrated a reduction in the abundance of pathogenic bacteria that are positively correlated with IBD progression after MMT-Fe@EcN treatment, as well as an increase in beneficial probiotic bacteria that aid in IBD recovery (Fig. 6G,H and Fig. S26). MMT-Fe@EcN regulates the gut microbiota by enhancing the colonization ability of EcN in the intestinal tract and by reducing H_2S levels to protect and repair the intestinal environment. These dual actions promote a healthier gut microbiome, which is crucial for overall intestinal health. In summary, these findings indicate that MMT-Fe@EcN holds promising potential in successfully restoring a healthy microbiota composition, providing valuable insights into its therapeutic benefits in the treatment of IBD.

3. Conclusions and discussion

The gut microbiota constitutes a large microbial community that has been shown to be crucial for maintaining host health [40–43]. The introduction of probiotics is often used as an attractive strategy for preventing and treating IBD, as it can reduce the colonization of pathogens and maintain a healthy microbial composition [31,32,44]. However, the success of microbial biotherapy relies on sufficient adherence and colonization of probiotics at the diseased intestinal site following oral administration. In inflamed areas, the mucosal layer becomes depleted and compromises the intestinal mucus barrier, significantly hindering the adhesion and colonization of orally administered probiotics. Various methods have been explored, such as using alginate salts, chitosan, dopamine, and other probiotic coatings, to enhance probiotic adhesion to the intestinal mucosa [12–14,45–47]. Nevertheless, existing probiotic delivery approaches mainly focus on enhancing interactions with intestinal mucus, which still face challenges in limited colonization efficacy in mucus-depleted inflammatory bowel segments during IBD. Moreover, the excessive production of H_2S in the inflamed sites further depleting the mucus layer and adversely affecting both probiotic colonization and IBD recovery [17,38,48]. Therefore, challenges remain in how to effectively deliver and colonize probiotics in mucus-depleted and inflammatory conditions.

Inspired by the strong intestinal adhesion ability of clinically approved MMT, we developed an oral probiotic delivery system, MMT-Fe@EcN, which effectively adheres to the site of inflammation and synergistically scavenges H_2S, resulting in success in the treatment of colitis. The core of the system revolves around the utilization of clinically proven montmorillonite as a safe carrier for efficient delivery of the clinical strain of probiotic EcN for colitis relief. Comprehensive investigations encompassing both in vitro and in vivo assessments validate the absence of systemic side effects following MMT-Fe@EcN treatment. In the context of mucus-depleted inflammatory lesions, characterized by a positive charge attributed to various cationic exudates [33,34], MMT-Fe@EcN leverages its strong adhesive capability and electronegativity to establish adherence. Simultaneously, the MMT-Fe component offers a

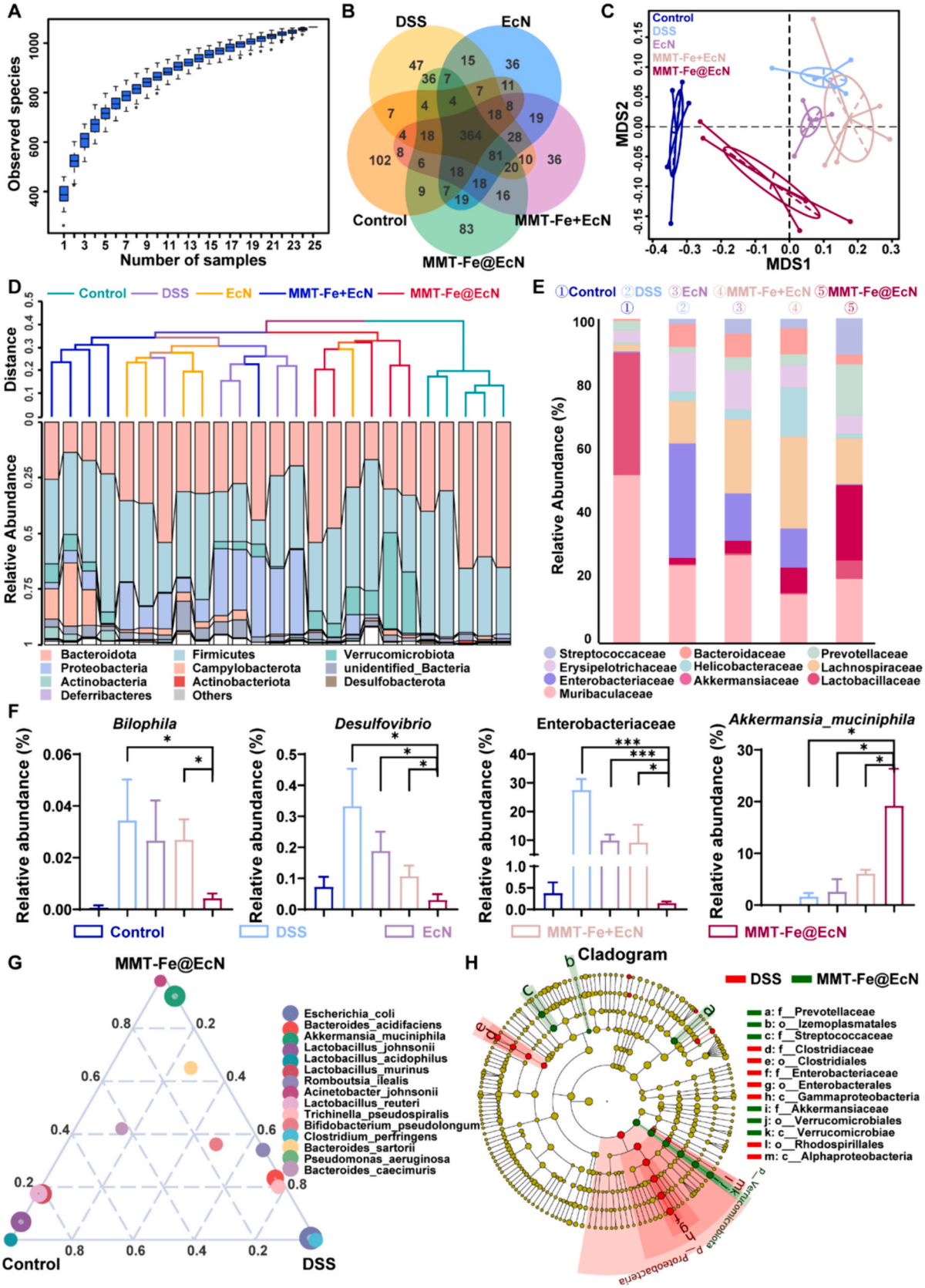

Fig. 6. MMT-Fe@EcN restores colitis-associated gut microbiota dysbiosis. A) Box plots demonstrate the accumulation of alpha-diverse species in the gut microbiota. B) Venn diagrams showing the differences in composition between different communities. C) NMDS plot visualizes the gut microbiome β-diversity, with each point representing one mouse. D) Dendrogram generated using UPGMA method. E) Relative abundance of bacteria classified at a family-level taxonomy. F) Relative abundance of select taxa. G) Effects of MMT-Fe@EcN on gut microbiota at a species level using the ternaryplot method. H) Linear discriminant analysis effect size for the DSS versus MMT-Fe@EcN comparison. Data are presented as the means ± SD (n = 5). $^{*}P < 0.05$, $^{**}P < 0.01$, $^{***}P < 0.001$ determined by Student's *t*-test.

dual benefit by effectively scavenging H_2S through both physical adsorption and chemical consumption. Excess H_2S in the intestinal lumen, produced by sulfate-reducing bacteria (SRB) metabolism, is closely associated with IBD. H_2S has the ability to disrupt the disulfide bonds of mucin polymers in the mucus layer, leading to reduced viscosity and increased mucus permeability, which can exacerbate intestinal barrier dysfunction [17,38,48]. Therefore, the H_2S scavenging property of MMT-Fe plays a crucial role in repairing the intestinal barrier and further enhances the colonization rate of probiotics in treating IBD.

Overall, MMT-Fe@EcN represents a promising and safe therapeutic strategy for the delivery of probiotics to diseased sites and the treatment of IBD. Its unique combination of water-impermeability, inflamed site adhesion, and in situ H_2S scavenging properties provide a comprehensive and effective solution for addressing the challenges posed by mucus-depleted and inflamed environments in the intestines. The successful results demonstrated in the DSS-induced mouse model of colitis further emphasize the potential of MMT-Fe@EcN as an innovative approach to manage and treat IBD effectively. Current therapeutic methods for IBD either involve immune response inhibition or antagonism of specific inflammatory mediators [20,49]. Probiotic therapy avoids the off-target systemic side effects that can be caused by conventional immunosuppressive drugs based on small molecules or biologics [50]. However, probiotics are not completely devoid of pathogenic traits [51,52]. Considering the vulnerability of the different populations consuming these probiotic strains, the safety of the EcN strains developed in this study needs to be thoroughly and systematically tested before clinical application. In conclusion, MMT-Fe@EcN plays a critical and complementary role in the multifaceted benefits of colitis, providing a convenient and powerful platform for the treatment of IBD.

4. Materials and methods

4.1. Materials and strains

The *Escherichia coli* Nissle 1917 strain was obtained from Beijing Baio Bowei Biotechnology Co., LTD. The plasmid pBBR1MCS2-Tac-mCherry (kanamycin resistant) and pUC19-EGFP (Ampicillin resistant) were purchased from Wuhan Miaoling Biotechnology Co., Ltd. Luria−Bertani (LB) agar and LB broth were obtained from Beijing Solaibao Technology Co., LTD. Montmorillonite powder was purchased from Bfu-Yipson (Tianjin) Pharmaceutical Co., Ltd. Anhydrous ferric chloride was acquired from Aladdin's official website. The H_2S content Assay Kit was purchased from Beijing Solaibao Technology Co., LTD. Additionally, the mouse hydrogen sulfide ELISA kit was obtained from Nanjing Camilo biological engineering Co., Ltd. The Live/dead staining kit was purchased from Shanghai Bestbio Co. DAPI was purchased from Wuhan Sunncell Biotechnology Co., Ltd. FITC was purchased from MedBio Pharmaceutical Technology. DSS was purchased from Yeasen Biotechnology (Shanghai) Co., Ltd.

4.2. Preparation of MMT-Fe@EcN

MMT-Fe was first prepared by the previous methods with some modifications in studies [53]. Firstly, MMT was prepared by stirring for 3 h at room temperature and then sonicated at 280 W for 20 min. Next, utilizing the adsorption capacity of MMT, 20 mg of ferric chloride was added to the MMT nanodispersion and stirred for 3 h at room temperature. After centrifugation, we obtained the MMT-Fe. Subsequently, the MMT-Fe was employed to coat the surface of EcN, harnessing its adsorption capacity and interactions, including van der Waals forces and hydrogen bonding. Briefly, a suspension of 1×10^8 bacterial cells in 1.5 mL of PBS was prepared, and then 2 mg mL^{-1} of MMT-Fe were added to the bacterial suspension at room temperature. After 2 h of stirring, the modified bacteria were obtained by centrifugation (5000 rpm, 6 min) and subsequently washed three times with PBS.

4.3. In vitro removal of H_2S

For the detection of H_2S, we employed WSP-1, which utilizes a reaction-based fluorescence turn-on strategy. WSP-1 selectively and rapidly reacts with H_2S to produce a fluorescent compound that emits yellow fluorescence at Ex 465 nm, and Em 515 nm. To assess the effectiveness of MMT-Fe@EcN in removing H_2S, we recorded the fluorescence spectra and intensity of the two groups using a fluorescence spectrophotometer. The first group consisted of 100 μL of WSP-1 (10 μM) added to 500 μL of sodium sulfide (50 μM) treated with 500 μL of MMT-Fe@EcN (2 mg mL^{-1}) for 1 min. The second group, which served as a control, included 500 μL of ultrapure water mixed with 500 μL of sodium sulfide (50 μM).

4.4. Characterization of MMT-Fe@EcN

Visualization of both EcN and MMT-Fe@ EcN were achieved using Transmission Electron Microscopy (FEI Talos F200 S, UK). Samples were deposited on carbon-coated copper grids, allowing them to dry at room temperature for 15 min before observation. Scanning Electron Microscopy (ZEISS 1550VP FESEM) was also utilized to visualize the morphology of the EcN and MMT-Fe@ EcN. Following centrifugation (4000 *g*, 5 min), the collected bacteria were washed three times with PBS and then fixed in a 2.5% glutaraldehyde solution at room temperature for 1 h. Subsequently, the bacteria underwent two additional PBS washes and were dehydrated in a series of ethanol concentrations (30%, 50%, 70%, 80%, 90%, and 100%) for 15 min each. The ζ potential and hydrodynamic size of MMT-Fe@EcN and EcN were determined using Dynamic Light Scattering with a Malvern Zetasizer Nano ZS (UK). Rhodamine B-labeled MMT-Fe was detected through Flow Cytometry (Beckman Cyto Flex, UK). Moreover, the coating of MMT-Fe on the surface of EcN was observed using Confocal Laser Scanning Microscopy (CLSM600, Sunny Optical Technology, China).

4.5. Growth of MMT-Fe@EcN

The EcN, MMT-Fe + EcN, and MMT-Fe@EcN were each diluted in LB medium to attain an initial bacterial concentration of 1×10^3 CFU. Subsequently, the diluted cultures were incubated at 37 °C with continuous shaking at 200 rpm. At 1-h intervals, the OD_{600} values of the cultures were measured using a microplate reader (BioTek, USA) within a 96-well plate, over 12 h.

Cell viability was assessed using CCK-8 (New Cell & Molecular Biotech, China). MMT-Fe@EcN, MMT-Fe + EcN, and EcN were diluted in LB medium to attain an initial bacterial concentration of 1×10^5 CFU. Subsequently, 190 μL of each cell culture was dispensed into a 96-well plate, and 10 μL of the CCK-8 solution was added. The plate was then incubated at 37 °C. At one-hour intervals, the OD values of the cultures were measured at 450 nm using a microplate spectrophotometer.

4.6. The resistance of MMT-Fe@EcN in simulated harsh environments

Equivalent MMT-Fe@EcN and EcN (1×10^8 CFUs) were resuspended in 1 mL of simulated gastric fluid (SGF) with a pH of 1.2, which included 20 mg sodium chloride, 32 mg pepsin, and 70 μL hydrochloric acid per 100 mL of deionized water, or in a solution of bile salts (0.3 mg mL^{-1}). The cultures were then incubated at 37 °C with continuous shaking at 200 rpm. At designated time intervals, 50 μL of each sample was extracted, washed with PBS, and plated onto solid LB agar plates. Subsequently, the plates were incubated overnight at 37 °C, and colony counting was carried out.

At the specified time points, 10 μL of each sample was collected for TEM observation. Furthermore, the use of live/dead staining kits allowed for the assessment of bacterial activity following various treatments.

Additionally, the probiotics were subjected to sequential incubation

in SGF for 1 h and bile salts for 2 h to better mimic the harsh gastrointestinal environment. Afterward, they were resuspended in a culture medium and gently shaken at 37 °C. The OD values at 600 nm were measured hourly to generate growth curves and monitor the viability and growth of the probiotics. To assess the stability of the MMT-Fe@EcN coatings after incubation in SGF and bile salts, rhodamine B-labeled MMT-Fe was detected using flow cytometry and CLSM.

4.7. MMT-Fe@EcN adhesion properties of lesions at simulated sites of inflammation

To create models of inflamed and healthy mucosa, polystyrene plates were coated with human recombinant transferrin (Sigma-Aldrich) or mucin from pig stomach (Sigma-Aldrich). For the transferrin coating, a concentration of 100 μg/mL in PBS was added to a 24-well polystyrene plate (Fisher Scientific) and left to incubate overnight at 37 °C to coat the surface. To coat with mucin, a 3% (*w/v*%) mucin solution in Hank's Balanced Salt Solution (HBSS, Invitrogen) was added to a second plate, and gentle shaking at room temperature was performed for 2 h.

Subsequently, the two modified plates were placed in a flow chamber. Rhodamine B (absin)-labeled MMT-Fe@EcN was introduced into the flow chamber and allowed to flow over the surfaces of the transferrin-coated and mucin-coated plates for a duration of 5 min. After the flow of MMT-Fe@EcN, the plates were carefully removed from the flow chamber and prepared for fluorescence imaging.

4.8. Animals

All animal experiments were conducted in accordance with the guidelines outlined in Zhengzhou University's Guide for the Care and Use of Laboratory Animals. Female C57BL/6 mice aged 6 weeks were provided by Beijing HFK Biosciences Co., Ltd. The animal license number is 110322211102955054, and the animal laboratory is accredited with the number SCXK (YU) 2020–0008.

4.9. CLSM observation of the distribution of MMT-Fe@EcN in the intestine

The intestinal tissues from healthy mice and mice with colitis were collected. One side of the tissues was ligated with a medical suture to create a small pocket. The tissues were then stained with FITC-WGA and slowly injected with a suspension of MMT-Fe@EcN-mCherry. Afterward, the tissues were incubated in PBS buffer at 37 °C for 30 min to allow for probiotic adhesion. Following the incubation period, the intestinal tissues were sectioned, and the sections were observed using CLSM.

4.10. Distribution of MMT-Fe@EcN in the gastrointestinal tract

The distribution of probiotics in the gastrointestinal tract after oral administration was observed using the small animal live imaging system (ami HTX, Spectral Instrument Image, USA). Twenty-four mice were randomly divided into two groups: EcN-GFP and MMT-Fe@EcN-GFP. Each mouse was administered a bacterial suspension containing 1×10^8 CFU of the respective probiotic. At specific time points (2 h, 12 h, 24 h, and 48 h) after administration, three mice from each group were euthanized, and their tissues were collected for imaging using the live imaging system.

4.11. Retention of MMT-Fe@EcN in the GI tract

The bacterial retention in the gastrointestinal tract was investigated in female C57BL/6 mice aged 6–8 weeks. At each time point, three mice from each group were used for the experiment. The mice were orally administered with the same dose of either EcN or MMT-Fe@EcN. After 4, 48, and 96 h of administration, the mice were euthanized, and the contents of their stomach, small intestine, colon, and cecum were collected. The collected samples were diluted in PBS and plated onto solid LB agar plates. The plates were then incubated overnight to allow for the growth and formation of bacterial colonies.

4.12. Long-term adherence of probiotics in the body

The mice were orally administered with 200 μL of either EcN-mCherry or MMT-Fe@EcN-mCherry (5×10^8 CFU mL^{-1}). On the 3rd and 6th day after administration, the mice were euthanized, and their colons were collected. Each colon was sectioned into 1 cm segments and frozen for sectioning at a depth of 10 μm. The tissue sections were then observed using CLSM to visualize the distribution of the bacteria in the colon.

4.13. Biosafety assessment

The mice received a daily administration of 200 μL of MMT-Fe@EcN and EcN (5×10^8 CFU mL^{-1}) for a total of 5 days and were sacrificed on the 5th day. Blood, heart, liver, spleen, lung, kidney, and intestinal tissue samples were collected from each mouse. These samples were then immersed in tissue fixation solution (1 mL per sample) and subjected to H&E staining to visualize and analyze tissue morphology.

In addition to histological analysis, liver function, kidney function, and blood routine parameters were assessed for each group of mice. These analyses provided valuable information about the impact of MMT-Fe@EcN and EcN administration on various organs and physiological parameters. For comparison, a control group of mice was included, which received no probiotic treatment, serving as the blank group.

4.14. Model of DSS-induced colitis

A mouse model was created using 6-week-old female C57BL/6 mice. The normal control group was provided with filtered sterile water, whereas the model group received water containing 3% DSS (molecular weight 36,000 - 50,000) for 7 days, followed by normal drinking water. Subsequently, the model group mice were randomly distributed into four groups: the model control group, EcN group, MMT-Fe group, MMT-Fe + EcN group, and MMT-Fe@EcN group. Each group received either 1×10^8 CFU of probiotics or PBS through oral administration for 5 consecutive days.

During the 12-day experimental period, the mice's daily body weight was closely monitored. On the final day of the experiment, feces were collected for microbiota analysis. At the conclusion of the study, the mice were humanely euthanized, and their entire colons were carefully extracted. The colon's length was measured, and it was gently rinsed with PBS. Two sections, each measuring 0.5 cm in length, were obtained from the distal end for histological evaluation (MPO antibody, Zen Bioscience) and immunofluorescence staining (ZO-1 antibody, Signalway Antibody; occludin-1 Aantibody, GeneTex). The level of apoptosis in colonic epithelial cells was evaluated in vivo. Briefly, the TUNEL assay (Keygen BioTECH) was performed to detect apoptosis in colon tissues according to the manufacturer's instructions [54]. Images were acquired by CLSM and Image J-NIH freeware to measure the intensity of staining. The ROS levels in colon tissues were further evaluated in vivo. Briefly, frozen sections are used to measure colon ROS levels with Dihydroethidium (MedChemExpress). Images were acquired by CLSM and Image J-NIH freeware to measure the intensity of staining.

4.15. Cytokine assays

Separate colon tissue samples were utilized to measure cytokine concentrations. Enzyme-linked immunosorbent Assay (ELISA) analysis was conducted for in vivo assessment. Commercial ELISA kits were employed to detect cytokines in both serum and tissue samples (IL-10 ELISA Kit, JLW20242, Jianglai biology, Shanghai;TNF-α ELISA KIT,

E04741m, CUSABIO, https://www.cusabio.com/; IL-6, IF N-γ, TGF-β ELISA Kit, Quanzhou jiubang Biotechnology Co., Ltd). To determine the cytokine concentrations in colon tissue, the colon segments were homogenized at a ratio of 1:10 (*w/v*) in 50 mM PBS (pH 6.0). Each sample was then subjected to centrifugation at 4 °C and 10,000 g for 10 min, and the resulting supernatant was collected for further analysis.

4.16. *In vivo H_2S scavenging*

To verify the effectiveness of MMT-Fe@EcN in reducing H_2S content, feces were collected after 5 days of treatment with EcN, MMT-Fe + EcN, and MMT-Fe@EcN, respectively. Feces collection involved picking up the feces of each group of mice in a timely manner, quickly weighing them, and placing them in an airtight container. The collected feces were stored in a − 80-degree refrigerator or liquid nitrogen for uniform measurement. H_2S levels in the colon and feces were detected using an H_2S ELISA kit (Camilo Bioengineering Co., Ltd., Nanjing, China).

4.17. *Bacteria translocation*

EcN was transfected with a plasmid expressing mCherry labeled with anti-kanamycin. DSS-induced mice were orally instilled with EcN or MMT-Fe@EcN doses (3×10^8 CFU in 150 μL PBS) for 5 consecutive days. To assess bacterial translocation, heart, liver, spleen, lung, and kidney tissues were collected separately at the end of the day. The tissues were further ground and diluted with 1 mL of PBS. A suspension of the tissue (40 μL) was applied to a selective solid LB plate (100 μg/mL kanamycin, MeilunBio). Bacteria were incubated overnight at 37 °C and counted.

4.18. *Microbiome analysis*

After different treatments in DSS-induced colitis-bearing mice, the feces were collected, and prepared for gut microbiome analysis by 16S sequencing assay. The 16S gene sequencing and analysis were conducted at Novogene Co., Ltd. Briefly, the total DNA was extracted (DC112, Vazyme, Nanjing, China) and sequenced by building a sequencing library on illumina NovaSeq. QPCR was used to detect the effective concentration of the library (SYBR qPCR SuperMix Plus, Cat. No.:E096, Novoprotein, Shanghai, China). The data analysis was performed on NovoMagic Plus. Venn Graph to analyze the results of each group of feature sequences; Species Accumulation Boxplot to analyze the adequacy of samples. Beta diversity was analyzed with nonmetric multidimensional scaling (NMDS) and UPGMA clustering analysis. Ternary plots and LDA effect size analyses were used to assess differences in dominant species between samples.

4.19. *Statistical analysis*

All data were expressed as mean ± SD. Differences considered statistically significant were performed by Student *t*-test of GraphPad Prism 8.02, ($^*P < 0.05$, $^{**}P < 0.01$, *and* $^{***}P < 0.001$).

CRediT authorship contribution statement

Jiali Yang: Writing – review & editing, Writing – original draft, Conceptualization. **Shengchan Ge:** Methodology, Investigation. **Shaochong Tan:** Investigation. **Hua Liu:** Methodology. **Mingzhu Yang:** Investigation. **Wei Liu:** Supervision. **Kaixiang Zhang:** Methodology. **Zhenzhong Zhang:** Supervision. **Junjie Liu:** Writing – review & editing. **Jinjin Shi:** Writing – review & editing, Conceptualization. **Zhi-Hao Wang:** Writing – review & editing. **Jitian Li:** Funding acquisition.

Declaration of competing interest

The authors declare no conflicts of interest.

Data availability

No data was used for the research described in the article.

Acknowledgments

This work was supported by the National Natural Science Foundation of China (Nos. 82222067, 82172762, 31900991, 21904119, 82073395); Science and technology innovation talents support project of Henan Province (No. 23HASTIT041), and Henan Provincial Science and Technology Research and Development Plan Joint Fund (No. 222301420050); Henan Science Fund for Outstanding Young Scholars (No. 232300421051, 222300420020); Postdoctoral Innovative Talent Support Program of Henan Province (No. ZYYCYU202012179); The Key Program of Superior Disciplines of Henan Province, (No. 222301420011); Henan University Science and Technology Innovation Team (No. 23IRTSTHN025); Key Research and Development Project in Henan Province (No. 231111310500); Young Elite Scientists Sponsorship Program by CAST (2021-QNRC2-A06). The authors would like to thank Shiyanjia Lab (www.shiyanjia.com) for the TEM analysis.

Appendix A. Supplementary data

Supplementary data to this article can be found online at https://doi.org/10.1016/j.jconrel.2024.07.071.

References

[1] T.E. Adolph, M. Meyer, J. Schwärzler, L. Mayr, F. Grabherr, H. Tilg, The metabolic nature of inflammatory bowel diseases, Nat. Rev. Gastroenterol. Hepatol. 19 (12) (2022) 753–767, https://doi.org/10.1038/s41575-022-00658-y.
[2] M. Cainzos-Achirica, K. Glassner, H.S. Zawahir, A.K. Dey, T. Agrawal, E.M. M. Quigley, B.P. Abraham, I. Acquah, T. Yahya, N.N. Mehta, K. Nasir, Inflammatory bowel disease and atherosclerotic cardiovascular disease: JACC review topic of the week, J. Am. Coll. Cardiol. 76 (24) (2020) 2895–2905, https://doi.org/10.1016/j.jacc.2020.10.027.
[3] E.C. Martens, M. Neumann, M.S. Desai, Interactions of commensal and pathogenic microorganisms with the intestinal mucosal barrier, Nat. Rev. Microbiol. 16 (8) (2018) 457–470, https://doi.org/10.1038/s41579-018-0036-x.
[4] G. Rook, F. Backhed, B.R. Levin, M.J. McFall-Ngai, A.R. McLean, Evolution, human-microbe interactions, and life history plasticity, Lancet 390 (10093) (2017) 521–530, https://doi.org/10.1016/S0140-6736(17)30566-4.
[5] A. Abdel-Gadir, E. Stephen-Victor, G.K. Gerber, M. Noval Rivas, S. Wang, H. Harb, L. Wang, N. Li, E. Crestani, S. Spielman, W. Secor, H. Biehl, N. DiBenedetto, X. Dong, D.T. Umetsu, L. Bry, R. Rachid, T.A. Chatila, Microbiota therapy acts via a regulatory T cell MyD88/RORgammat pathway to suppress food allergy, Nat. Med. 25 (7) (2019) 1164–1174, https://doi.org/10.1038/s41591-019-0461-z.
[6] C.G. Buffie, V. Bucci, R.R. Stein, P.T. McKenney, L. Ling, A. Gobourne, D. No, H. Liu, M. Kinnebrew, A. Viale, E. Littmann, M.R. van den Brink, R.R. Jenq, Y. Taur, C. Sander, J.R. Cross, N.C. Toussaint, J.B. Xavier, E.G. Pamer, Precision microbiome reconstitution restores bile acid mediated resistance to Clostridium difficile, Nature 517 (7533) (2015) 205–208, https://doi.org/10.1038/nature13828.
[7] T. Nakatsuji, T.R. Hata, Y. Tong, J.Y. Cheng, F. Shafiq, A.M. Butcher, S.S. Salem, S. L. Brinton, A.K. Rudman Spergel, K. Johnson, B. Jepson, A. Calatroni, G. David, M. Ramirez-Gama, P. Taylor, D.Y.M. Leung, R.L. Gallo, Development of a human skin commensal microbe for bacteriotherapy of atopic dermatitis and use in a phase 1 randomized clinical trial, Nat. Med. 27 (4) (2021) 700–709, https://doi.org/10.1038/s41591-021-01256-2.
[8] D.W. Zheng, X. Dong, P. Pan, K.W. Chen, J.X. Fan, S.X. Cheng, X.Z. Zhang, Phage-guided modulation of the gut microbiota of mouse models of colorectal cancer augments their responses to chemotherapy, Nat. Biomed. Eng. 3 (9) (2019) 717–728, https://doi.org/10.1038/s41551-019-0423-2.
[9] Y. Yu, S. Lin, Z. Chen, B. Qin, Z. He, M. Cheng, M. Sun, J. Sun, Bacteria-driven biotherapy: from fundamental studies to clinical trials, Nano Today 48 (2023) 101731.
[10] A.S. Luis, G.C. Hansson, Intestinal mucus and their glycans: a habitat for thriving microbiota, Cell Host Microbe 31 (7) (2023) 1087–1100, https://doi.org/10.1016/j.chom.2023.05.026.
[11] G.M.H. Birchenough, M.E.V. Johansson, Forming a mucus barrier along the colon, Science 370 (6515) (2020) 402–403, https://doi.org/10.1126/science.abe7194.
[12] X. Wang, Z. Cao, M. Zhang, L. Meng, Z. Ming, J. Liu, Bioinspired oral delivery of gut microbiota by self-coating with biofilms, Sci. Adv. 6 (26) (2020) eabb1952, https://doi.org/10.1126/sciadv.abb1952.
[13] Y. Liu, B. Liu, D. Li, Y. Hu, L. Zhao, M. Zhang, S. Ge, J. Pang, Y. Li, R. Wang, P. Wang, Y. Huang, J. Huang, J. Bai, F. Ren, Y. Li, Improved gastric acid resistance and adhesive colonization of probiotics by Mucoadhesive and intestinal targeted

Konjac Glucomannan microspheres, Adv. Funct. Mater. 2001157 (2020), https://doi.org/10.1002/adfm.202001157.
[14] A.C. Anselmo, K.J. McHugh, J. Webster, R. Langer, A. Jaklenec, Layer-by-layer encapsulation of probiotics for delivery to the microbiome, Adv. Mater. 28 (43) (2016) 9486–9490, https://doi.org/10.1002/adma.201603270.
[15] Y. Dou, P. Liu, Z. Ding, Y. Zhou, H. Jing, Y. Ren, Z. Heger, V. Adam, N. Li, Orally administrable H(2) S-scavenging metal-organic framework prepared by co-flow microfluidics for comprehensive restoration of intestinal milieu, Adv. Mater. 35 (14) (2023) e2210047, https://doi.org/10.1002/adma.202210047.
[16] I. Kushkevych, D. Dordevic, M. Vitezova, Possible synergy effect of hydrogen sulfide and acetate produced by sulfate-reducing bacteria on inflammatory bowel disease development, J. Adv. Res. 27 (2021) 71–78, https://doi.org/10.1016/j.jare.2020.03.007.
[17] D. Dordevic, S. Jancikova, M. Vitezova, I. Kushkevych, Hydrogen sulfide toxicity in the gut environment: Meta-analysis of sulfate-reducing and lactic acid bacteria in inflammatory processes, J. Adv. Res. 27 (2021) 55–69, https://doi.org/10.1016/j.jare.2020.03.003.
[18] B.D. Paul, S.H. Snyder, K. Kashfi, Effects of hydrogen sulfide on mitochondrial function and cellular bioenergetics, Redox Biol. 38 (2021) 101772, https://doi.org/10.1016/j.redox.2020.101772.
[19] Z. Al Nabhani, S. Dulauroy, E. Lecuyer, B. Polomack, P. Campagne, M. Berard, G. Eberl, Excess calorie intake early in life increases susceptibility to colitis in adulthood, Nat. Metab. 1 (11) (2019) 1101–1109, https://doi.org/10.1038/s42255-019-0129-5.
[20] G. Lin, F. Yu, D. Li, Y. Chen, M. Zhang, K. Lu, N. Wang, S. Hu, Y. Zhao, H. Xu, Polydopamine-cladded montmorillonite micro-sheets as therapeutic platform repair the gut mucosal barrier of murine colitis through inhibiting oxidative stress, Mater. Today Bio. 20 (2023) 100654, https://doi.org/10.1016/j.mtbio.2023.100654.
[21] D. Nguyen-Thanh, K. Block, T.J. Bandosz, Adsorption of hydrogen sulfide on montmorillonites modified with iron, Chemosphere 59 (3) (2005) 343–353, https://doi.org/10.1016/j.chemosphere.2004.10.022.
[22] K. Stepova, D. Maquarrie, I. Krip, Modified bentonites as adsorbents of hydrogen sulfide gases, Appl. Clay Sci. 42 (3–4) (2009) 625–628, https://doi.org/10.1016/j.clay.2008.05.001.
[23] M. Akbari Alavijeh, M.N. Sarvi, Z. Ramazani Afarani, Properties of adsorption of vitamin B12 on nanoclay as a versatile carrier, Food Chem. 219 (2017) 207–214, https://doi.org/10.1016/j.foodchem.2016.09.140.
[24] A. Troge, W. Scheppach, B.O. Schroeder, S.A. Rund, K. Heuner, J. Wehkamp, E. F. Stange, T.A. Oelschlaeger, More than a marine propeller–the flagellum of the probiotic *Escherichia coli* strain Nissle 1917 is the major adhesin mediating binding to human mucus, Int. J. Med. Microbiol. 302 (7–8) (2012) 304–314, https://doi.org/10.1016/j.ijmm.2012.09.004.
[25] S. Stebe-Frick, M.J. Ostaff, E.F. Stange, N.P. Malek, J. Wehkamp, Histone deacetylase-mediated regulation of the antimicrobial peptide hBD2 differs in intestinal cell lines and cultured tissue, Sci. Rep. 8 (1) (2018) 12886, https://doi.org/10.1038/s41598-018-31125-x.
[26] P. Praveschotinunt, A.M. Duraj-Thatte, I. Gelfat, F. Bahl, D.B. Chou, N.S. Joshi, Engineered E. Coli Nissle 1917 for the delivery of matrix-tethered therapeutic domains to the gut, Nat. Commun. 10 (1) (2019) 5580, https://doi.org/10.1038/s41467-019-13336-6.
[27] C.B. Kurtz, Y.A. Millet, M.K. Puurunen, M. Perreault, M.R. Charbonneau, V. M. Isabella, J.W. Kotula, E. Antipov, Y. Dagon, W.S. Denney, D.A. Wagner, K. A. West, A.J. Degar, A.M. Brennan, P.F. Miller, An engineered E. Coli Nissle improves hyperammonemia and survival in mice and shows dose-dependent exposure in healthy humans, Sci. Transl. Med. 11 (475) (2019), https://doi.org/10.1126/scitranslmed.aau7975.
[28] V.M. Isabella, B.N. Ha, M.J. Castillo, D.J. Lubkowicz, S.E. Rowe, Y.A. Millet, C. L. Anderson, N. Li, A.B. Fisher, K.A. West, P.J. Reeder, M.M. Momin, C.G. Bergeron, S.E. Guilmain, P.F. Miller, C.B. Kurtz, D. Falb, Development of a synthetic live bacterial therapeutic for the human metabolic disease phenylketonuria, Nat. Biotechnol. 36 (9) (2018) 857–864, https://doi.org/10.1038/nbt.4222.
[29] J. Yang, G. Zhang, X. Yang, M. Peng, S. Ge, S. Tan, Z. Wen, Y. Wang, S. Wu, Y. Liang, J. An, K. Zhang, J. Liu, J. Shi, Z. Zhang, An oral "super probiotics" with versatile self-assembly adventitia for enhanced intestinal colonization by autonomous regulating the pathological microenvironment, Chem. Eng. J. 446 (2022) 137204, https://doi.org/10.1016/j.cej.2022.137204.
[30] X. Yang, J. Yang, Z. Ye, G. Zhang, W. Nie, H. Cheng, M. Peng, K. Zhang, J. Liu, Z. Zhang, J. Shi, Physiologically inspired mucin coated Escherichia coli Nissle 1917 enhances biotherapy by regulating the pathological microenvironment to improve intestinal colonization, ACS Nano (2022), https://doi.org/10.1021/acsnano.1c09681.
[31] H. Luo, Y. Chen, X. Kuang, X. Wang, F. Yang, Z. Cao, L. Wang, S. Lin, F. Wu, J. Liu, Chemical reaction-mediated covalent localization of bacteria, Nat. Commun. 13 (1) (2022) 7808, https://doi.org/10.1038/s41467-022-35579-6.
[32] Z. Cao, X. Wang, Y. Pang, S. Cheng, J. Liu, Biointerfacial self-assembly generates lipid membrane coated bacteria for enhanced oral delivery and treatment, Nat. Commun. 10 (1) (2019) 5783, https://doi.org/10.1038/s41467-019-13727-9.
[33] C.J. Edmonds, Electrical potentials of the sigmoid colon and rectum in irritable bowel syndrome and ulcerative colitis, Gut 11 (10) (1970) 867–874, https://doi.org/10.1136/gut.11.10.867.
[34] L. Hong, G. Chen, Z. Cai, H. Liu, C. Zhang, F. Wang, Z. Xiao, J. Zhong, L. Wang, Z. Wang, W. Cui, Balancing microthrombosis and inflammation via injectable protein hydrogel for inflammatory bowel disease, Adv. Sci. 9 (20) (2022) e2200281, https://doi.org/10.1002/advs.202200281.
[35] S. Zhang, J. Ermann, M.D. Succi, A. Zhou, M.J. Hamilton, B. Cao, J.R. Korzenik, J. N. Glickman, P.K. Vemula, L.H. Glimcher, G. Traverso, R. Langer, J.M. Karp, An inflammation-targeting hydrogel for local drug delivery in inflammatory bowel disease, Sci. Transl. Med. 7 (300) (2015) 300ra128, https://doi.org/10.1126/scitranslmed.aaa5657.
[36] M. Perse, A. Cerar, Dextran sodium sulphate colitis mouse model: traps and tricks, J. Biomed. Biotechnol. 2012 (2012) 718617, https://doi.org/10.1155/2012/718617.
[37] Q. Song, H. Zhao, C. Zheng, K. Wang, H. Gao, Q. Feng, H. Zhang, Z. Zhang, Y. Zhang, L. Wang, A bioinspired versatile spore coat nanomaterial for Oral probiotics delivery, Adv. Funct. Mater. (2021) 2104994, https://doi.org/10.1002/adfm.202104994.
[38] N. Ijssennagger, C. Belzer, G.J. Hooiveld, J. Dekker, S.W. van Mil, M. Muller, M. Kleerebezem, R. van der Meer, Gut microbiota facilitates dietary heme-induced epithelial hyperproliferation by opening the mucus barrier in colon, Proc. Natl. Acad. Sci. USA 112 (32) (2015) 10038–10043, https://doi.org/10.1073/pnas.1507645112.
[39] Y. Lee, K. Sugihara, M.G. Gillilland 3rd, S. Jon, N. Kamada, J.J. Moon, Hyaluronic acid-bilirubin nanomedicine for targeted modulation of dysregulated intestinal barrier, microbiome and immune responses in colitis, Nat. Mater. 19 (1) (2020) 118–126, https://doi.org/10.1038/s41563-019-0462-9.
[40] R. Caruso, B.C. Lo, G. Nunez, Host-microbiota interactions in inflammatory bowel disease, Nat. Rev. Immunol. 20 (7) (2020) 411–426, https://doi.org/10.1038/s41577-019-0268-7.
[41] Y. Zhang, C.X. Li, X.Z. Zhang, Bacteriophage-mediated modulation of microbiota for diseases treatment, Adv. Drug Deliv. Rev. 176 (2021) 113856, https://doi.org/10.1016/j.addr.2021.113856.
[42] Z. Li, Y. Wang, J. Liu, P. Rawding, J. Bu, S. Hong, Q. Hu, Chemically and biologically engineered Bacteria-based delivery systems for emerging diagnosis and advanced therapy, Adv. Mater. 33 (38) (2021) e2102580, https://doi.org/10.1002/adma.202102580.
[43] N. Li, L. Wang, L. Li, M.-Z. Yang, Q.-X. Wang, X.-W. Bai, F. Gao, Y.-Q. Yuan, Z.-J. Yu, Z.-G. Ren, The correlation between gut microbiome and atrial fibrillation: pathophysiology and therapeutic perspectives, Mil. Med. Res. 10 (1) (2023) 51, https://doi.org/10.1186/s40779-023-00489-1.
[44] P. Feng, Z. Cao, X. Wang, J. Li, J. Liu, On-demand bacterial reactivation by restraining within a triggerable nanocoating, Adv. Mater. (2020) e2002406, https://doi.org/10.1002/adma.202002406.
[45] C. Pan, J. Li, W. Hou, S. Lin, L. Wang, Y. Pang, Y. Wang, J. Liu, Polymerization-mediated multifunctionalization of living cells for enhanced cell-based therapy, Adv. Mater. (2021) e2007379, https://doi.org/10.1002/adma.202007379.
[46] D. Wei, Y. Sun, H. Zhu, Q. Fu, Stimuli-responsive polymer-based nanosystems for cancer theranostics, ACS Nano 17 (23) (2023) 23223–23261, https://doi.org/10.1021/acsnano.3c06019.
[47] T. Wei, S. Thakur, M. Liu, J. Wen, Oral delivery of glutathione: antioxidant function, barriers and strategies, Materia. Medica 1 (2022) 177–192, https://doi.org/10.15212/AMM-2022-0005.
[48] N. Ijssennagger, R. van der Meer, S.W.C. van Mil, Sulfide as a mucus barrier-breaker in inflammatory bowel disease, Trends Mol. Med. 22 (3) (2016) 190–199, https://doi.org/10.1016/j.molmed.2016.01.002.
[49] Y. Tian, J. Xu, Y. Li, R. Zhao, S. Du, C. Lv, W. Wu, R. Liu, X. Sheng, Y. Song, X. Bi, G. Li, M. Li, X. Wu, P. Lou, H. You, W. Cui, J. Sun, J. Shuai, F. Ren, B. Zhang, M. Guo, X. Hou, K. Wu, L. Xue, H. Zhang, M.V. Plikus, Y. Cong, C.J. Lengner, Z. Liu, Z. Yu, MicroRNA-31 reduces inflammatory signaling and promotes regeneration in colon epithelium, and delivery of mimics in microspheres reduces colitis in mice, Gastroenterology 156 (8) (2019) 2281–2296, https://doi.org/10.1053/j.gastro.2019.02.023.
[50] J. Zhou, M. Li, Q. Chen, X. Li, L. Chen, Z. Dong, W. Zhu, Y. Yang, Z. Liu, Q. Chen, Programmable probiotics modulate inflammation and gut microbiota for inflammatory bowel disease treatment after effective oral delivery, Nat. Commun. 13 (1) (2022) 3432, https://doi.org/10.1038/s41467-022-31171-0.
[51] J. Liu, Y. Wang, W.J. Heelan, Y. Chen, Z. Li, Q. Hu, Mucoadhesive probiotic backpacks with ROS nanoscavengers enhance the bacteriotherapy for inflammatory bowel diseases, Sci. Adv. 8 (45) (2022) eabp8798, https://doi.org/10.1126/sciadv.abp8798.
[52] D. Pradhan, R.H. Mallappa, S. Grover, Comprehensive approaches for assessing the safety of probiotic bacteria, Food Control 108 (2020) 106872, https://doi.org/10.1016/j.foodcont.2019.106872.
[53] J. Kim, S.P. Hlaing, J. Lee, A. Saparbayeva, S. Kim, D.S. Hwang, E.H. Lee, I.-S. Yoon, H. Yun, M.-S. Kim, H.R. Moon, Y. Jung, J.-W. Yoo, Exfoliated bentonite/alginate nanocomposite hydrogel enhances intestinal delivery of probiotics by resistance to gastric pH and on-demand disintegration, Carbohydr. Polym. 272 (2021) 118462, https://doi.org/10.1016/j.carbpol.2021.118462.
[54] D. Wei, J. Fan, J. Yan, C. Liu, J. Cao, C. Xu, Y. Sun, H. Xiao, Nuclear-targeting lipid Pt(IV) prodrug Amphiphile cooperates with siRNA for enhanced cancer immunochemotherapy by amplifying Pt-DNA adducts and reducing phosphatidylserine exposure, J. Am. Chem. Soc. 146 (1) (2024) 1185–1195, https://doi.org/10.1021/jacs.3c12706.